

Effect of Alloying Elements on The Corrosion Behavior of 0Cr12Ni3Co12Mo4W Ultra High Strength Stainless Steel

Huiyan Li¹, Chaofang Dong^{1,*}, Kui Xiao¹, Xiaogang Li¹, Pin Zhong²

¹ Corrosion and Protection Center, Key Laboratory for Corrosion and Protection (MOE), University of Science and Technology Beijing, Beijing 100083, China

² Beijing Institute of Aeronautical Materials, Beijing 100095, China

*E-mail: cfdong@ustb.edu.cn

Received: 30 August 2015 / Accepted: 15 October 2015 / Published: 4 November 2015

The effect of alloying elements on the corrosion behavior of 0Cr12Ni3Co12Mo4W ultra high strength stainless steel (UHSS) in 0.1M Na₂SO₄ solutions with Cl⁻ at pH=3 was studied by XPS, AES, SEM, EDS and a series of electrochemical measurements. The passive film with a thickness of about 7nm, formed on the UHSS surface in 0.1M Na₂SO₄ solution at pH=3, contained an outer layer as n-type semiconductor with Fe₃O₄ and NiO, and an inner layer as p-type semiconductor with Cr₂O₃. The electrochemical measurements results showed that two kinds of pitting corrosion, outer pitting and inner pitting, occurred on the surface of UHSS specimens in 0.1M Na₂SO₄ + 1wt.% NaCl solution at pH=3. The outer corrosion products were mainly composed of the oxides of Fe, Cr, Mo and Co, while the inner corrosion products were mainly composed of the oxides of Cr and Mo. During the inner pitting corrosion, the alloying elements Fe and Co were dissolved and diffused out of the pits, while Cr and Mo were dissolved and then deposited in the pits.

Keywords: ultra high strength stainless steel, passive film, alloying element, XPS, AES

1. INTRODUCTION

High strength stainless steels with excellent mechanical properties and moderate corrosion resistance are suitable for a wide range of applications such as steam generators, pressure vessels, cutting tools, and offshore plate forms for oil extraction [1-6]. Their properties can be changed by additive alloying elements, such as Cr, Mn, and Co improving the strength and toughness, Ni and Mo improving the toughness, Ti improving the strength but reducing the toughness [7-11]. Martin et al. [12] studied that the effect of alloying elements on hydrogen environment embrittlement of AISI type 304 austenitic stainless steel, and the results showed that the material's ductility was improved by increasing the Si, Mn and Cr content. Sugimoto et al. [13] reported that Nb addition of 0.08% in

0.2%C-1.5%Si-1.5%Mn-0.02-0.11%Nb TRIP-aided sheet steels achieved the best combination of total elongation and stretch-flange ability, accompanied with an increase in peak austempering temperature for total elongation. Xu et al. [14] reported that B, Ce and N can improve the creep life of the type-347H austenitic stainless steel significantly at high temperature.

The effect of alloying elements on the corrosion behavior of stainless steels is an important issue to provide guidance to the material design and usage in industry field. Farahat et al. [15] reported that the influence of hot forging and alloying with Al on the electrochemical behavior and mechanical properties of austenitic stainless steel, and the results showed that Al alloying increased the work-hardening property and deteriorated the ductility due to decreasing the austenite phase and increasing the ferrite phase, but had an adverse effect on the pitting corrosion resistance. Rovere et al. [16] reported that the best corrosion behavior of the shape memory stainless steels in acid media was shown by the shape memory stainless steel that contained the highest amount of Cr and the lowest amount of Mn. The beneficial effect of Cr was to promote the formation of a compact Cr_2O_3 film and the detrimental effect of Mn was related to its low passivity coefficient, reducing the activity of Cr-adsorbed species and also to the formation of unstable Mn oxides. The balance between the Cr and Mn contents played an important role in the corrosion behavior. Zhou et al. [17] studied the effects of Cr, Ni and Cu on the corrosion behavior of low carbon microalloying steel in a Cl^- containing environment, and the results showed that Cr concentrated mainly in the inner region of the rust of Cr-Ni-Cu steel, inner/outer interface especially, whereas Ni was uniformly distributed all over the rust and Cu was noticed rarely. The addition of Cr and Ni was beneficial to the formation of dense and compact inner rust layer, which was the most important reason for the improvement of corrosion resistance of experimental steel. Fernengel et al. [18] reported that the addition of Co affected the corrosion resistance of sintered Nd-Fe-B magnets, and 3.5 at.% Co additions were required for an improved corrosion stability for sintered Nd-Fe-B magnets. Therefore, the effect of alloying elements which play an important role in improving the mechanical properties of ultra high strength stainless steels on the corrosion behavior is necessary to be studied.

The purpose of this work was to investigate how the alloying elements affect the corrosion behavior of a novel ultra high strength stainless steel. X-ray photoelectron spectroscopy (XPS) and Auger electron spectroscopy (AES) were carried out to represent the composition and depth distribution of elements in the passive film. The semiconductor properties of the passive films were tested by Mott-Schottky method. Additionally, Potentiostatic electrochemical measurements were used to determinate the electrochemical properties of specimens in 0.1M Na_2SO_4 solution with Cl^- . Finally, the elements distribution in the inner and outer corrosion products were also explored by energy dispersive spectroscopy (EDS).

2. EXPERIMENTS

2.1 Specimens and solution

A novel ultra high strength stainless steel (UHSSS for short) 0Cr12Ni3Co12Mo4W with chemical composition listed in Table 1 was used in this study. The UHSSS plate was heated to

austenitizing temperature 1080°C, quenched by oil to room temperature, followed by cooled to -73°C for 1 hour to transform retained austenite and finally tempered at 600°C for 4 hours. The schematic of the heat treatment process was showed in Fig. 1.

Table 1. Chemical composition of the ultra high strength stainless steel (wt.%)

Element										
	C	Cr	Co	Mo	Ni	W	V	Ti	Si	Mn
Wt.%	0.089	12.41	12.3	4.43	2.59	0.98	0.24	<0.005	0.053	<0.10

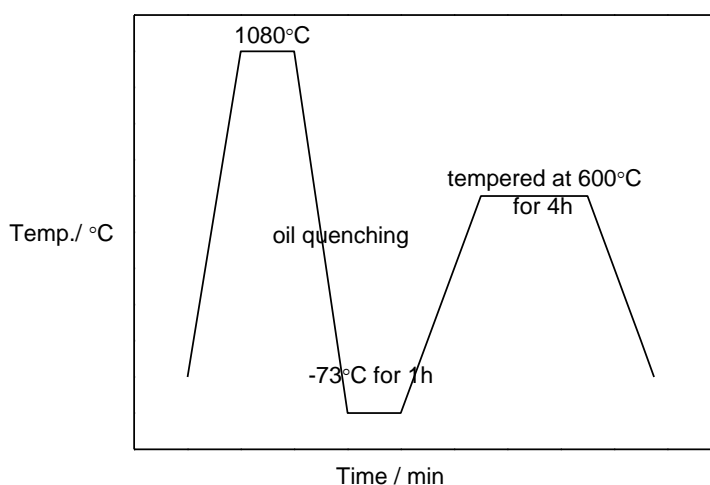


Figure 1. Schematic of heat treatment process.

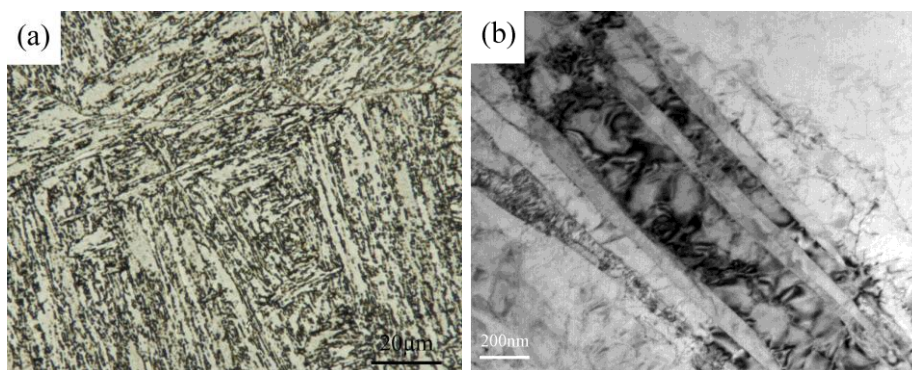


Figure 2. Microstructure (a) and TEM image (b) of the UHSS.

Microstructure and TEM image of the novel UHSS are shown in Fig. 2. The microstructure consisted of lath/plant martensite with carbides distributed within the matrix and at the boundaries and

some retained austenite. Before the tests, specimens with a dimension of 10mm × 10mm × 3mm were cut from the steel plate and ground subsequently up to 2000 grit SiC paper and polished.

The test solution was 0.1M (Na₂SO₄ + H₂SO₄) solution prepared by distilled water and analytic grade reagents. The chloride ion concentration contained in the solution was 1wt.% by adding NaCl. The pH of the solution was adjusted by H₂SO₄.

2.2 Passive film analysis

The specimens were polarized at 0.6V_{SCE} in 0.1M Na₂SO₄ solution at pH=3 for 5 hours in a conventional three-electrode cell using a M370 advanced electrochemical system to form passive film. The Mott-Schottky plots were obtained by sweeping at a frequency of 1000Hz with an amplitude signal of 10mV, the potential ranging from -0.6V_{SCE} to 1.5V_{SCE} and the potential step 50mV.

The specimens were then cleaned with distilled water and dried. The elements composition of the surface passive film was analyzed by XPS using a Fisons Escalab 250 spectrometer, with an unmonochromatized Al K α X-ray source ($h\nu=1486.6\text{eV}$). The source was operated at 15kV and 20mA. The binding energy scale was calibrated with the C 1s (284.5eV). Spectra of Fe 2p_{3/2}, Cr 2p_{3/2}, Ni 2p_{3/2}, Mo 3d_{5/2}, Co 2p_{3/2} and O 1s were recorded. The evaluation of the spectra was performed using the parameters of standard peaks.

AES analysis was performed to represent the depth profiles by a PHI model Auger Nanoprobe system (5kV electron beam operating at around 1 μ A, with a tilt of 30° of normal) produced by Japan ULVAC-PHI company. The pressure inside the chamber was around 3.9 × 10⁻⁹ Torr. Spectra were collected using coaxial electron gun and CMA energy analyzer. The sputtering rate was 3.4nm/min for SiO₂.

2.3 Electrochemical measurements

All specimens were embedded in epoxy resin leaving a working area of 1 cm², grounded to 1000 grit and cleaned by ethanol and deionized water prior to tests. The solution was 0.1M Na₂SO₄ + 1wt.% NaCl with pH=3, and all the tests were carried out at room temperature. The electrochemical measurements were performed in a conventional three-electrode cell using a M370 advanced electrochemical system. The test specimen was used as the working electrode, a platinum sheet as the counter electrode, and all potentials were measured against a saturated calomel electrode (SCE) connected to the cell via a Luggin probe.

Prior to electrochemical measurements, working electrodes were initially reduced potentiostatically at -1.2V_{SCE} for 3min to remove air-formed oxides. EIS measurement was performed with applied potential amplitude of 10mV at the open circuit potential in the frequency range of 100kHz to 10mHz. The polarization curves were measured potentiodynamically from -0.3V (vs. corrosion potential E_{corr}) to 1.8V_{SCE} with a scanning rate of 0.5mV/s.

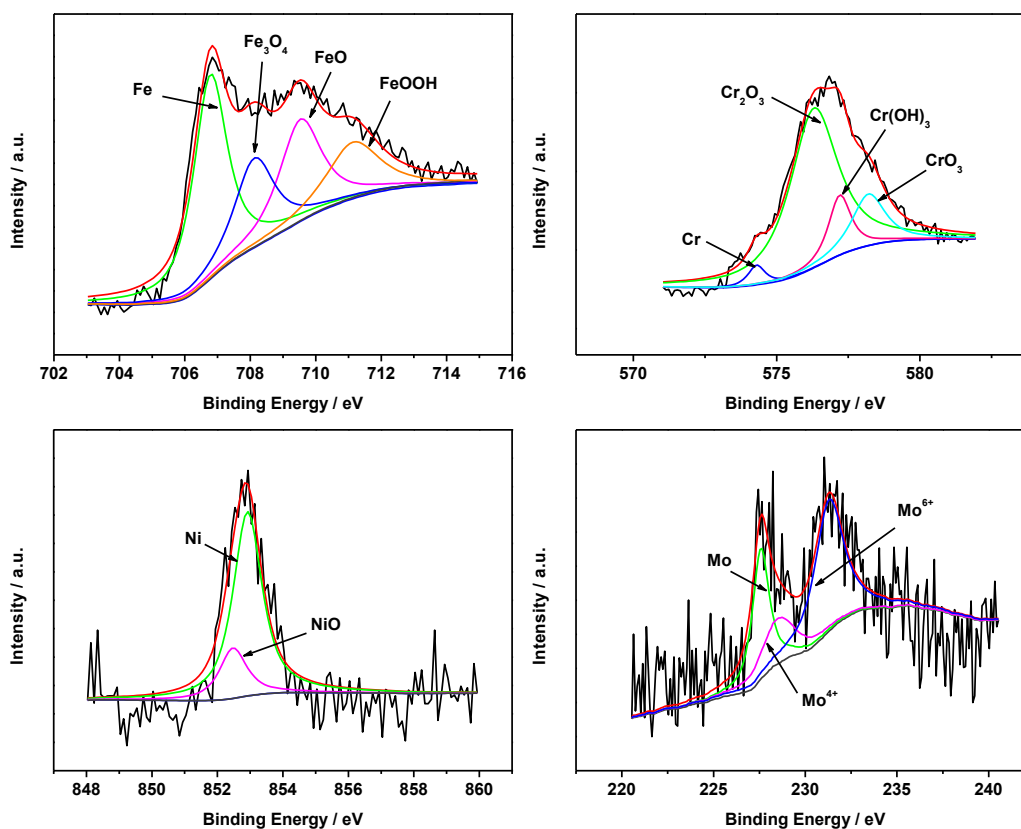
2.4 Scanning electron microscopy (SEM) and energy dispersive X-ray spectroscopy (EDS) analysis

After electrochemical measurements, the surface morphology of the steel electrode was observed using an FEI Quanta250 environmental scanning electron microscope (SEM) with an energy dispersive spectroscopy (EDS) system. EDS analysis was used to characterize the elemental distribution of the outer and inner corrosion products.

3. RESULTS AND DISCUSSION

3.1 The composition of the passive film

XPS measurement was carried out to characterize the composition of the passive film on the specimen formed in 0.1M Na₂SO₄ solution at pH=3. Fig. 3 showed the spectra of Fe 2p_{3/2}, Cr 2p_{3/2}, Ni 2p_{3/2}, Mo 3d_{5/2}, Co 2p_{3/2} and O 1s XPS signals on the surface of the passive film. The decomposition and fitting of the spectra was performed according to the parameters of standard peaks. The alloying element Fe mainly formed oxides of Fe, such as Fe₃O₄, FeO and FeOOH. In center of the Cr 2p_{3/2} peak regions, peaks due to Cr₂O₃ was strongly observed at 576.5eV [19]. The intensity of the Cr(OH)₃ and CrO₃ spectra was negligible.



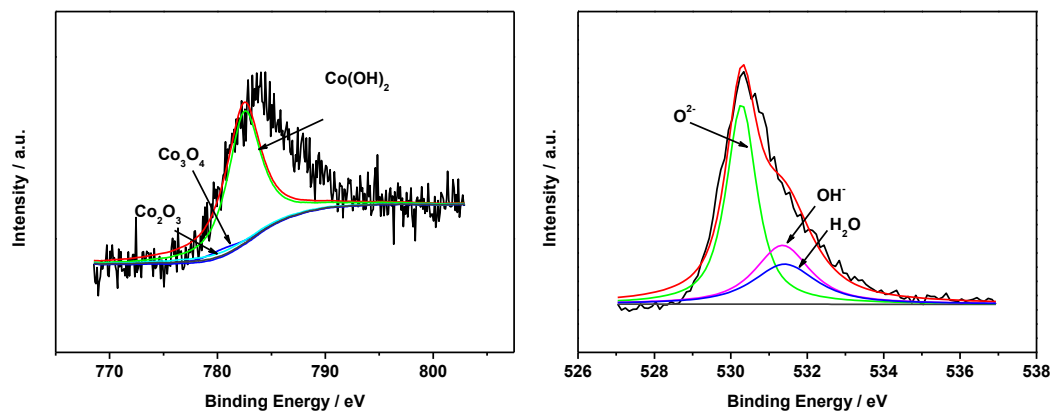


Figure 3. XPS spectra Fe 2p_{3/2}, Cr 2p_{3/2}, Ni 2p_{3/2}, Mo 3d_{5/2}, Co 2p_{3/2} and O 1s detected for the passive film formed on the UHSSS specimen in 0.1M Na₂SO₄ solution at pH=3.

For the alloying element Ni, the peak at 854eV can be assigned to Ni oxides such as NiO [20-22]. The preferentially formation of NiO led to the intensity of the metallic part of the spectrum gradually decreasing. Both the Co and Mo signals were quite low. For Mo, a peak at 228.8eV corresponded to the metallic species of Mo, and a peak at 232.5eV to the formation of MoO₃ [23]. For Co, it mainly formed Co(OH)₂ with the peak located at the binding energy 782eV.

It was suggested that the passive film on the UHSSS surface was mainly composed of Fe₃O₄, FeOOH, Cr₂O₃, NiO and MoO₃. Many literatures have confirmed that the passive film on stainless steel consisted of an inner layer of Cr₂O₃ and an outer layer of Fe₃O₄ [24, 25].

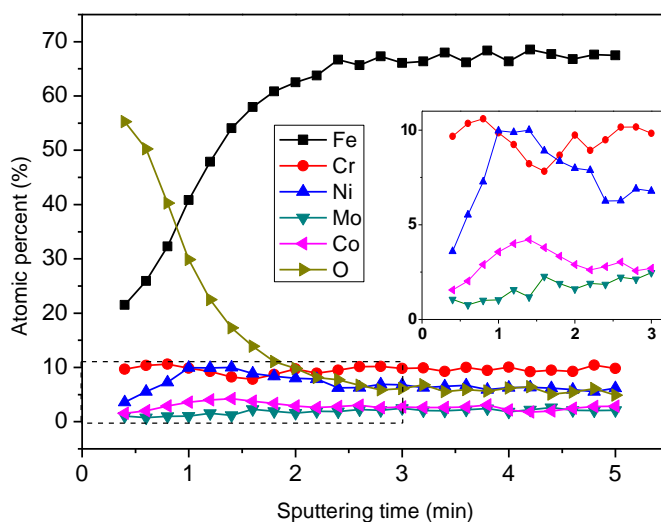


Figure 4. AES depth profiles for the passive film of the UHSSS formed in 0.1M Na₂SO₄ solution at pH=3.

To further understand the characters of the passive film, AES measurement was carried out to characterize the composition of the passive film on the specimen formed in 0.1M Na₂SO₄ solution at

pH=3. Fig. 4 showed the composition as a function of sputtering time for the passive film on the UHSSS formed in 0.1M Na₂SO₄ solution at pH=3. It was evident that in the passive film formed on the UHSSS specimen surface, the Fe content in the film was obviously lower than in the steel substrate. The Cr and Mo contents in the film were a little lower than in the steel substrate. On the contrast, the Ni and Co contents in the film were higher than in the steel substrate. Previous works have reported that passive films formed by selective dissolution, as the ions migrating under control of an electric field. Fe migrated faster through the film and dissolved preferentially at the outer film interface, leaving a film enriched in Cr, so passive films were normally enriched in Cr with a thickness of 1-5nm. For most stainless steels with Fe, Cr and Ni as the main alloying elements, as the oxidation of Fe and Cr, Ni remained enriched in its metallic state immediately below the film. As the primary passive element, the enrichment of Cr in passive films increased the corrosion resistance of the films [26, 27]. Mo accelerated the formation of stable passive film enriched with oxide of Cr, and prevented the dissolution of the steel.

It was reported that the passive film on stainless steel consisted of an outer layer of oxides of Fe and an inner layer of oxides of Cr [24]. The details of the elements depth composition were also shown in Fig. 4. It could be observed that Ni and Co contents were higher in the outer layer than in the inner layer [28]. Mo content was low both in the inner layer and outer layer. It was suggested that the passive film of the UHSSS consisted of an inner layer of oxides of Cr and an outer layer of oxides of Fe and a bit of oxides of Ni and Co. According to the XPS results, the inner layer mainly consisted of Fe₃O₄, FeOOH, NiO and MoO₃, and the inner layer mainly consisted of Cr₂O₃.

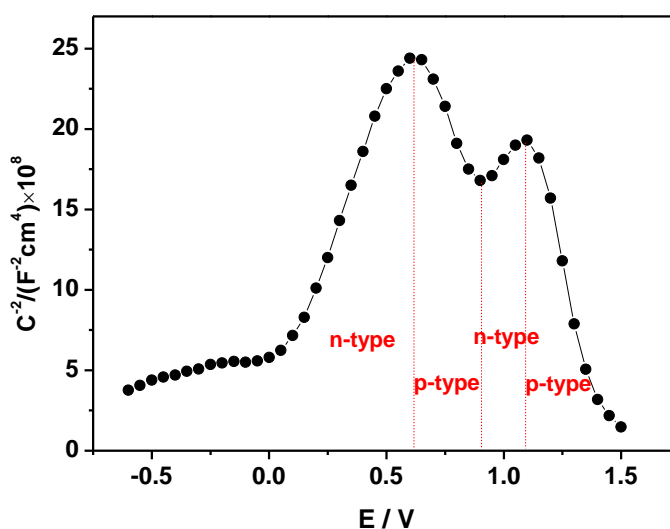


Figure 5. Mott-Schottky plots for the UHSSS in 0.1M Na₂SO₄ solution at pH=3.

As the sputtering rate was 3.4nm/min, a relative thickness of the passive film could be determined by measuring the sputtering time, was about 7nm. May et al. [29] reported that the thickness of the passive film of martensitic stainless steel X12CrNiMoV12-3 was approximately 3nm

for the passive film formed in air and 7nm for the passive film formed in the aqueous solution. Jung et al. [24] reported that the thickness of the passive films on Type 304 stainless steel surface in humid atmosphere was about 1~3nm. The previous works have reported that the most passive films of stainless steels were about 1~5nm. The thickness of the UHSSS formed in 0.1M Na₂SO₄ solution at pH=3 was relatively thicker, and it was an important factor for improving the corrosion resistance.

Fig. 5 showed the Mott-Schottky plots for UHSSS in 0.1M Na₂SO₄ solution at pH=3. The slopes of the curve turned at potentials 0.6V, 0.9V and 1.0V. From 0V to 0.6V, the oxide film on the specimen performed n-type semiconductor property. At the potential ranging between 0.6V and 0.9V, the passive film performed p-type semiconductor property due to the negative slope. Such variation of n-type to p-type repeatedly appeared at potentials from 0.9V to 1.0V and from 1.0V to 1.5V. The repeated shift phenomenon was probably caused by the composition and structure of passive film [30].

According to recent researches on the semiconductor properties of passive films on stainless steels, the oxides were considered as n-type semiconductor such as Fe₂O₃, MoO₃ and FeOOH, while it was considered as p-type semiconductor such as Cr₂O₃, NiO, MoO₂, FeCr₂O₄, etc [30]. According to the analysis of the XPS results, the passive film on the specimen was composed of Cr₂O₃, Fe₃O₄, FeOOH, NiO and MoO₃. In combination with the AES depth profiles, it could be concluded that the passive film of UHSSS formed in 0.1M Na₂SO₄ solution at pH=3 consisted of an outer layer as n-type semiconductor with Fe₃O₄, FeOOH, NiO and MoO₃, and an inner layer as p-type semiconductor with Cr₂O₃.

3.2 Electrochemical properties of the UHSSS

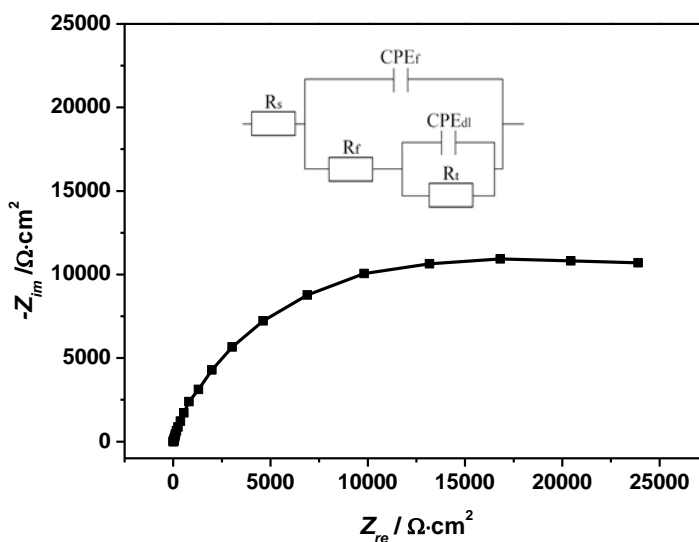


Figure 6. EIS result of the UHSSS specimen in 0.1M Na₂SO₄ + 1wt.% NaCl solution at pH=3.

Fig. 6 showed EIS results of the UHSSS specimen in 0.1M Na₂SO₄ + 1wt.% NaCl solution at pH=3 with only a capacitive reactance arc. The electrochemical equivalent circuits was also showed in

Fig. 6, where R_s was the solution resistance, CPE_f was the double-charge layer capacitance, R_f was charge-transfer resistance, CPE_{dl} was the capacitance of the corrosion product formed on the electrode surface, and R_t was resistance of corrosion product. It has been proposed and accepted in other researches, for example, the electrochemical equivalent circuit of Aermet100 ultra high strength steel in 0.5M Na_2SO_4 solution at pH=3 [31], and 316L austenitic stainless steel in 0.6g/L Cl^- solution [32].

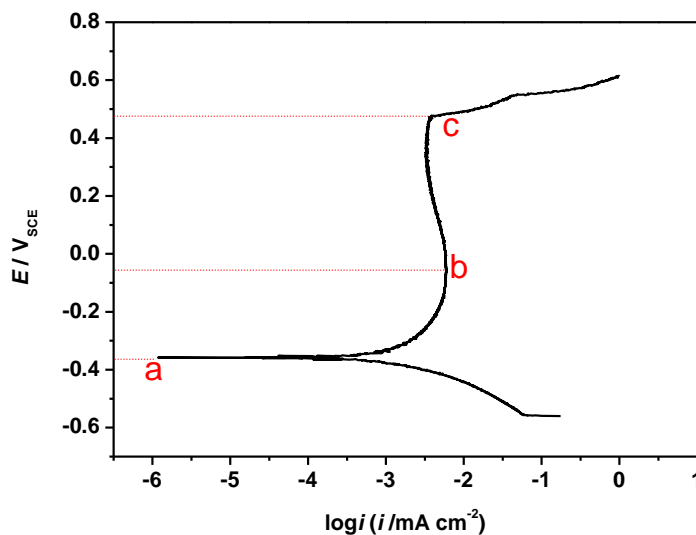
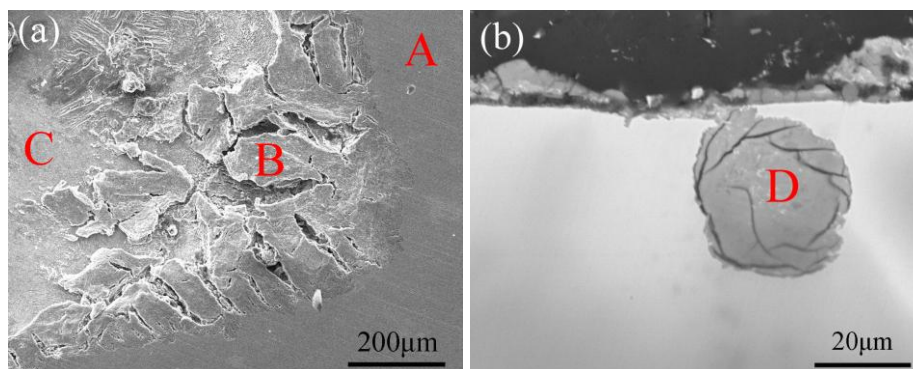


Figure 7. The potentiodynamic polarization curve of the UHSSS specimen in 0.1M Na_2SO_4 + 1wt.% NaCl solution at pH=3.

Table 2. Values of the parameters observed from polarization curve in Fig. 7

$E_{corr} / \text{mV vs. SCE}$	$I_{corr} / \mu\text{A}$	$\beta_c / \text{mV vs. SCE}$	$\beta_a / \text{mV vs. SCE}$
-380.6	2.7	78.2	126.1



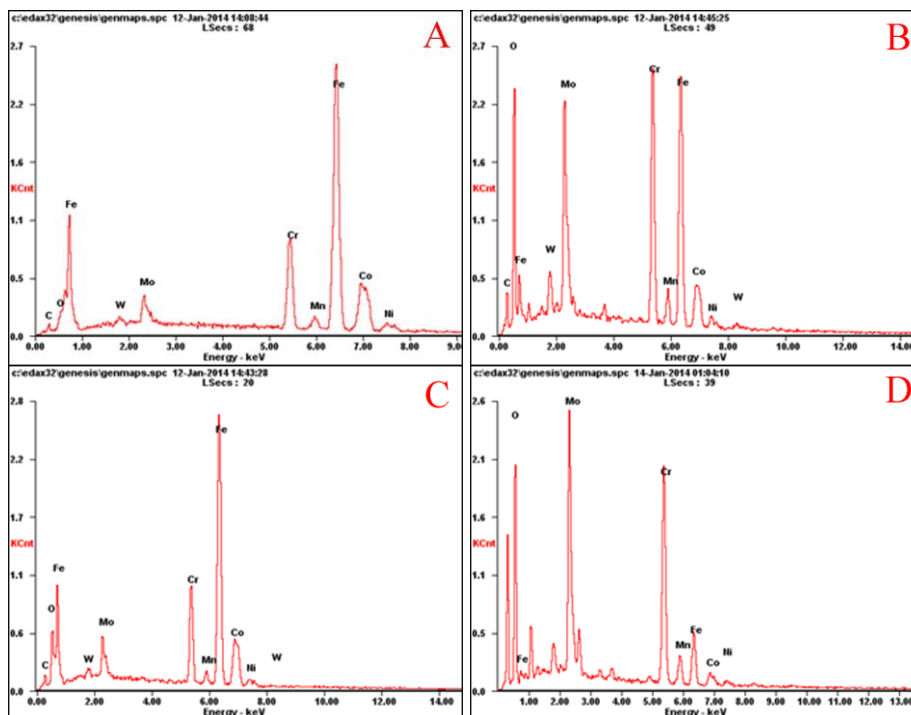


Figure 8. Microstructure and EDS analysis of UHSSS: (a) surface; (b) cross section.

Fig. 7 showed the potentiodynamic polarization curve of the UHSSS specimen measured in 0.1M Na₂SO₄ + 1wt.% NaCl solution at pH=3. It could be seen that the corrosion potential for the specimen was about -0.37V, which was relatively lower than most of other stainless steel in some hard environment [33-35], the passive potential section was from -0.05V to 0.48V, and the pitting potential was 0.48V, which is relatively higher [31, 36].

The values of the electrochemical parameters observed from polarization curve in Fig. 7. It can be seen that the corrosion resistance of UHSSS was wonderful for the value of corrosion current density i_{COR} was low, just 2.7μA. The anodic Tafel slope β_a is larger than the cathodic Tafel slope β_c , so the electrochemical reaction of the UHSSS in 0.1M Na₂SO₄ + 1wt.% NaCl solution at pH=3 was controlled by anodic reation.

The results showed that the UHSSS was more sensitive to corrosion, but with wide passive potential section and difficult to occur pitting corrosion. The microstructures of the specimen after electrochemical tests in 0.1M Na₂SO₄ + 1wt.% NaCl solution at pH=3 were shown in Fig. 8. It was pitting corrosion that occurred on the surface of the UHSSS.

3.3 Corrosion products analysis

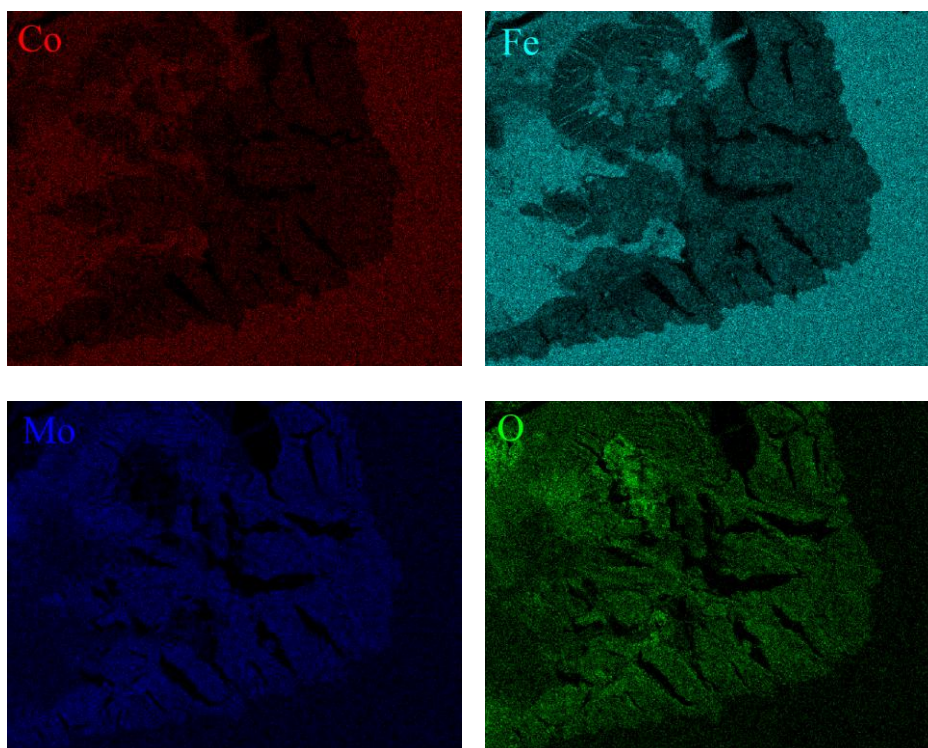
The microstructures of the surface and cross section of the specimens after electrochemical measurements in 0.1M Na₂SO₄ + 1wt.% NaCl solution at pH=3 were shown in Fig. 8. Some macroscopic pits with a diameter of 1~2mm were found on the surface of the specimens and some microscopic pits with a diameter of 10~100μm below the corrosion products were observed at the

cross section. The marked areas in Fig. 8 were respectively steel substrate (A), corrosion products part (B), corrosion products spalling part (C) and inner corrosion pit (D).

Table 3. The elements composition of the marked areas (At.%)

	Element							
	C K	O K	Fe K	Cr K	Co K	Mo K	Ni K	Mn K
A	8.11	5.68	54.51	12.51	12.80	2.59	2.52	0.66
B	18.23	32.63	20.26	14.95	4.78	6.34	1.56	0.49
C	12.41	13.85	46.20	11.52	10.13	2.90	2.15	0.44
D	--	56.69	6.75	21.78	1.82	11.43	0.91	0.63

The EDS analysis of the marked areas were also shown in Fig. 8 and the elements composition of the marked areas were listed in Table 3. It could be observed that the corrosion products was mainly composed of Fe, Cr and Mo, and the inner corrosion pit was mainly composed of Cr and Mo. The amounts of Cr and Mo in the inner corrosion pit were higher than in the surface corrosion products, but the amount of Fe in the inner corrosion pit was lower. It was suggested that the alloying elements Fe and Co were dissolved and diffused out of the pits, while Cr and Mo were dissolved and then deposited in the pits.



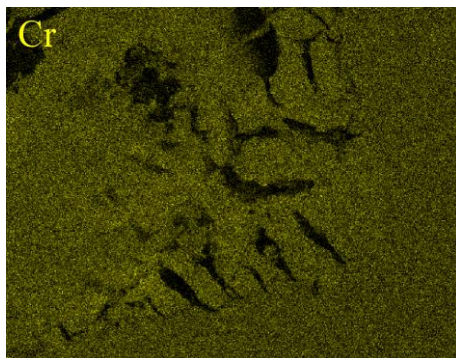
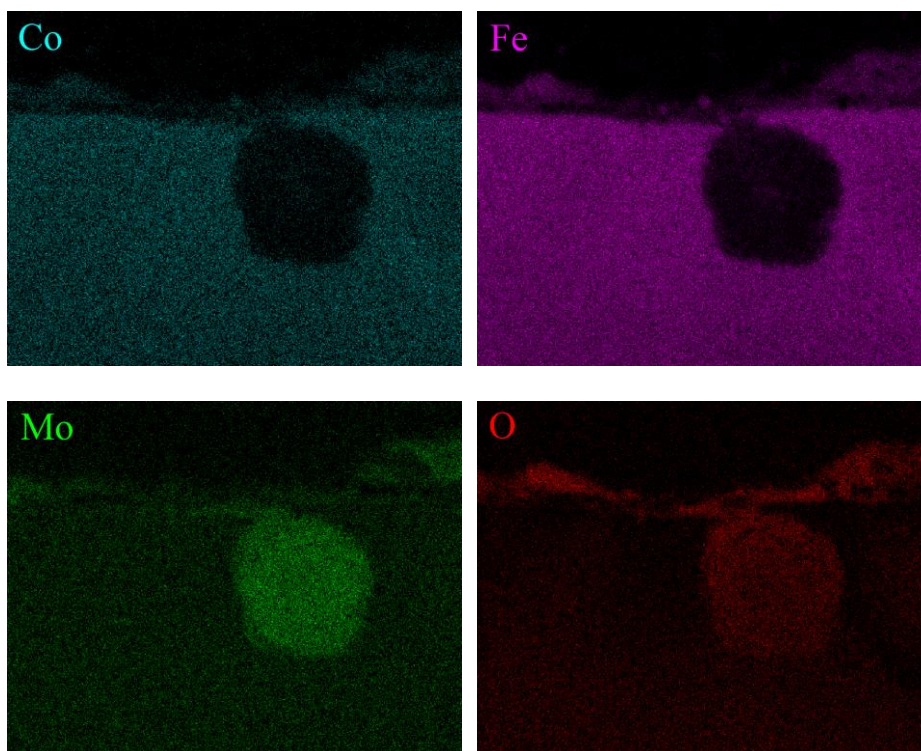


Figure 9. Elements distribution on the surface of the UHSSS specimen using EDS mapping after the electrochemical measurement (Fig. 8(a) showed the SEM image of this area on the same scale as the EDS maps).

The empirical pitting resistance equivalent number (PREN) of stainless steels could be calculated according to the Eq.(1). The PREN value of the UHSSS was about 27. It was suggested that the amount of Cr, Mo and N was the final factor to the pitting resistance of the UHSSS.

$$PREN = wt.\% Cr + 3.3 \times wt.\% Mo + (16 \text{ to } 30) \times wt.\% N \quad (1)$$

EDS maps for the individual elements were shown in Fig. 9 and clearly demonstrated their distribution into distinct sections, corrosion products part, steel substrate and corrosion products spalling part.



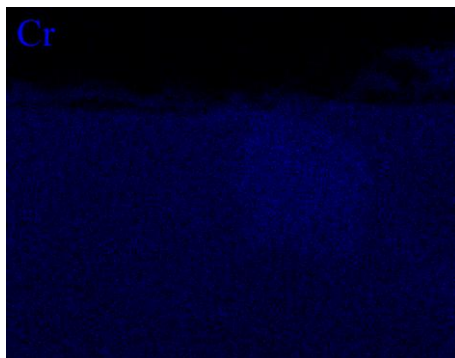


Figure 10. Elements distribution on the cross section of the UHSSS specimen using EDS mapping after electrochemical measurement (Fig. 8(b) showed the SEM image of this area on the same scale as the EDS maps).

The distributions of Cr were almost the same in all sections. The amounts of Mo and O in corrosion products part and corrosion products spalling part were larger than steel substrate. Mo was contributed to the corrosion behavior of the UHSSS. By contrast, smaller amount of Fe and Co was concentrated in the corrosion products than the other two sections. It was suggested that Fe and Co was contributed to inhibit corrosion behavior of the UHSSS, which is similar to the previous works of other stainless steels [37].

EDS maps for the individual elements in cross section were shown in Fig. 10 and clearly demonstrated their distribution into distinct sections, inner corrosion pit part, steel substrate and outer corrosion products part.

The elements maps in Fig. 10 indicated that the inner and outer corrosion products parts were both enriched in Cr, Mo and O. The corrosion products consisted of oxides of Cr and Mo. For the amount of Fe and Co, the inner and outer corrosion products were different. The amount of Fe and Co in outer corrosion products was smaller than that in steel substrate, but larger than in inner corrosion products part. It was suggested that Fe and Co were dissolved and diffused quickly during the corrosion process. In addition, the amounts of Cr and Mo in inner corrosion products part were a little larger than in the other sections. It was suggested that Cr and Mo were dissolved and then deposited in the pits.

4. CONCLUSIONS

The effect of alloying elements on the corrosion behavior of 0Cr12Ni3Co12Mo4W ultra high strength stainless steel in 0.1M Na₂SO₄ solutions with Cl⁻ at pH=3 has been investigated. The following conclusions could be drawn based on the results obtained:

(1) The passive film with a thickness of about 7nm, formed on the UHSSS surface in 0.1M Na₂SO₄ solution at pH=3 mainly consisted of an inner layer of oxides of Cr and an outer layer of oxides of Fe and a little of oxides of Ni and Mo.

(2) The electrochemical measurements results showed that the pitting corrosion occurred on the

UHSSS specimens in 0.1M Na₂SO₄ + 1wt.% NaCl solution at pH=3. The E_{corr} is about -0.37V and the E_p is about 0.48V. It was suggested that the UHSSS was more sensitive to corrosion, but with wide passive potential section and difficult to occur pitting corrosion.

(3) The microstructures and EDS maps of the specimen after electrochemical tests showed that the outer corrosion products were mainly composed of the oxides of Fe, Cr, Mo and Co, and the inner corrosion products were the oxides of Cr and Mo. It was suggested that the alloying elements Fe and Co were quickly dissolved and diffused out of the pits, while Cr and Mo were dissolved and then deposited in the pits.

ACKNOWLEDGMENTS

This work is supported by the National Natural Science Foundation of China (No.51171023), the Beijing Municipal Commission of Education (No. 00012134), the Fundamental Research Funds for the Central Universities (No. FRF-TP-14-011C1) and National Basic Research Program of China (973 Program) (No. 2014CB643300).

References

1. A. Isfahany, H. Saghafian and G. Borhani, *J. Alloys Compd.*, 509 (2011) 3931.
2. Z. Zhang, Z. Wang, Y. Jiang, H. Tan, D. Han, Y. Guo and J. Li, *Corros. Sci.*, 62 (2012) 42.
3. R. Fan, M. Gao, Y. Ma, X. Zha, X. Hao and K. Liu, *J. Mater. Sci. Technol.*, 28 (2012) 1059.
4. O. Akgun, M. Urgen and A. Cakir, *Mater. Sci. Eng., A*, 203 (1995) 324.
5. A. Pfennig, P. Zastrow and A. Kranzmann, *Int. J. Greenh. Gas Con.*, 15 (2013) 213.
6. J. Liu, G. Li, B. Peng and X. Zhang, *J. Iron Steel Res., Int.*, 14 (2007) 310.
7. M. Egawa, N. Ueda, K. Nakata, M. Tsujikawa and M. Tanaka, *Surf. Coat. Technol.*, 205 (2010) 5246.
8. D. Oh, K. Han, S. Hong and C. Lee, *Procedia Eng.*, 10 (2011) 383.
9. D. Oh, K. Han, S. Hong and C. Lee, *Mater. Sci. Eng., A*, 555 (2012) 44.
10. D. Han, Y. Jiang, C. Shi, Z. Li and J. Li, *Corros. Sci.*, 53 (2011) 3796.
11. T. Michler, J. Naumann and E. Sattler, *Int. J. Hydrogen Energy*, 37 (2012) 12765.
12. M. Martin, S. Weber, W. Theisen, T. Michler and J. Naumann, *Fuel Energy Abstr.*, 36 (2011) 15888.
13. K. Sugimoto, T. Muramatsu, S. Hashimoto and Y. Mukai, *J. Mater. Proc. Technol.*, 177 (2007) 390.
14. Y. Xu, H. Nie, J. Li, X. Xiao, C. Zhu and J. Zhao, *Mater. Sci. Eng., A*, 528 (2010) 643.
15. A. Farahat and A. Hamdy, *Mater. Des.*, 57 (2014) 538.
16. C. Rovere, J. Alano, J. Otubo and S. Kuri, *J. Alloys Compd.*, 509 (2011) 5376.
17. Y. Zhou, J. Chen, Y. Xu and Z. Liu, *J. Mater. Sci. Technol.*, 29 (2013) 168.
18. W. Fernengel, W. Rodewald, R. Blank, P. Schrey, M. Katter and B. Wall, *J. Magn. Magn. Mater.*, 196-197 (1999) 288.
19. K. Asami and K. Hashimoto, *Corros. Sci.*, 17 (1977) 559.
20. P. Marcus and J.M. Grimal, *Corros. Sci.*, 35 (1992) 805.
21. N. McIntyre, T. Rummery, M. Cook and D. Owen, *J. Electrochem. Soc.*, 123 (1976) 1164.
22. D. Singh and M. Banerjee, *Corrosion*, 42 (1986) 156.
23. A. Kocijan, C. Donik and M. Jenko, *Corros. Sci.*, 49 (2007) 2083.
24. R. Jung, H. Tsuchiya and S. Fujimoto, *Corros. Sci.*, 58 (2012) 62.
25. C. Olsson and D. Landolt, *Electrochim. Acta*, 48 (2003) 1093.

26. P. Ju, Y. Zuo, Y. Tang and X. Zhao, *Corros. Sci.*, 66 (2013) 330.
27. M. Pang, D. Bahr, D. Eakins and M. Norton, *Corrosion*, 57 (2001) 523.
28. S. Fajardo, D. Bastidas, M. Ryan, M. Criado, D. McPhail and J. Bastidas, *Appl. Surf. Sci.*, 256 (2010) 6139.
29. M. May, T. Palin-Luc, N. Saintier and O. Devos, *Inter. J. Fatigue*, 47 (2013) 330.
30. Z. Feng, X. Cheng, C. Dong, L. Xu and X. Li, *Corros. Sci.*, 52 (2010) 3646.
31. Y. Hu, C. Dong, M. Sun, K. Xiao, P. Zhong and X. Li, *Corros. Sci.*, 53 (2011) 4159.
32. J. Ding, L. Zhang, M. Lu, J. Wang, Z. Wen and W. Hao, *Appl. Surf. Sci.*, 289 (2014) 33.
33. C. Martins, J. Moreira and J. Martins, *Eng. Fail. Anal.*, 39 (2014) 65.
34. R. Moser, P. Singh, L. Kahn and K. Kurtis, *Corros. Sci.*, 57 (2013) 241.
35. J. Xu, X. Wu and E. Han, *Corros. Sci.*, 53 (2011) 1537.
36. G. Ilevbare and G. Burstein, *Corros. Sci.*, 45 (2003) 1545.
37. Y. Choi, J. Shim and J. Kim, *Mater. Sci. Eng., A*, 385 (2004) 148.

© 2015 The Authors. Published by ESG (www.electrochemsci.org). This article is an open access article distributed under the terms and conditions of the Creative Commons Attribution license (<http://creativecommons.org/licenses/by/4.0/>).